Geophysical Journal International

*Geophys. J. Int.* (2015) **203,** 2261–2276 doi: 10.1093/gji/ggv423
GJI Seismology

# Scattering of trapped *P* and *S* waves in the hydrated subducting crust of the Philippine Sea plate at shallow depths beneath the Kanto region, Japan

Shunsuke Takemura,[1,*] Kazuo Yoshimoto[2] and Takashi Tonegawa[3]

[1]*Earthquake Research Institute, University of Tokyo,* 1-1-1 *Yayoi, Bunkyo-ku, Tokyo* 113-0032*, Japan. E-mail: shunsuke@bosai.go.jp*
[2]*Department of Materials System Science, Graduate School of Nanobioscience, Yokohama City University,* 22-2 *Seto, Kanazawa-ku, Yokohama* 236-0027*, Japan*
[3]*Research and Development Center for Earthquake and Tsunami, Japan Agency for Marine-Earth Science and Technology,* 3173-25 *Showa-machi, Kanazawa-ku, Yokohama* 236-0001*, Japan*

Accepted 2015 September 29. Received 2015 September 29; in original form 2015 July 6

## SUMMARY

We performed a detailed analysis of seismograms obtained during intraslab earthquakes beneath the Kanto region and revealed a strong lateral variation in the waveforms of high-frequency trapped *P* and *S* waves propagating through the subducting crust of the Philippine Sea plate. Significantly distorted spindle-shaped trapped *P* and *S* waves with large peak delays were observed in areas where the Philippine Sea plate is at shallow depths beneath the Kanto region. In order to interpret these seismic observations, in relation to the structural properties of the crust of the Philippine Sea plate, we conducted finite difference method simulations of high-frequency seismic wave propagation using various possible heterogeneous velocity structure models. Our simulation successfully reproduced the observed characteristics of the trapped waves and demonstrated that the propagation of high-frequency *P* and *S* waves is significantly affected by small-scale velocity heterogeneities in the subducting crust. These heterogeneities can be traced to a depth of approximately 40 km, before disappearing at greater depths, a phenomenon that may be related to dehydration in the subducting crust at shallower depths.

**Key words:** Guided waves; Seismic attenuation; Computational seismology; Wave scattering and diffraction; Wave propagation.

## 1 INTRODUCTION

The hydrated oceanic crust, which is a low-velocity layer located in the uppermost part of a subducting oceanic plate, plays an important role in fluid transportation into the mantle (e.g. Peacock 1993; Iwamori & Zhao 2000; Abers 2005; Kawakatsu & Watada 2007). Fluid transportation due to subduction may be linked to various geophysical phenomena in subduction zones, such as the generation of arc volcanism and the occurrence of intraslab earthquakes (e.g. Tatsumi 1989; Kirby *et al*. 1996). In order to obtain better insight into the subsurface heterogeneous structures in subduction zones, numerous seismological surveys have been carried out in various subduction zones (e.g. Bostock *et al*. 2002; Matsubara *et al*. 2005; Rondenay *et al*. 2008; Nakajima *et al*. 2009a,b; Sodoudi *et al*. 2011; Liu & Zhao 2015). Their results and interpretations have contributed to understanding of fluid transportation around the slabs.

Previous seismic surveys and geochemical studies have revealed that hydrous minerals in the oceanic crust become unstable with increasing temperature and pressure due to subduction, and then dehydration reactions in the oceanic crust are expected to occur, accompanied by the release of fluids into surrounding structures, resulting in its transformation into an anhydrous eclogitic oceanic crust (e.g. Hacker *et al*. 2003; Kawakatsu & Watada 2007; Tsuji *et al*. 2008; Kuwatani *et al*. 2011).

In the subduction zone, where various heterogeneous structures related to the subduction of the oceanic plate can be found, several seismic later phases are often observed during intraslab earthquakes (e.g. Fukao *et al*. 1983; Martin & Rietbrock 2006; Miyoshi & Ishibashi 2007; Kennett & Furumara 2008; Hayashida *et al*. 2010; Miyoshi *et al*. 2012; Chen *et al*. 2013; Shiina *et al*. 2013, 2014). The study of seismic later phases potentially allows the investigation of seismological structures around the subducting oceanic plate. The trapped *P* and *S* waves, which propagate through the low-velocity oceanic crust and appear several seconds after the arrival of the relatively weak direct body waves, are usually observed at seismic stations on the fore-arc side of the subduction

[*] Now at: National Research Institute for Earth Science and Disaster Prevention, 3-1 Tennodai, Tsukuba, Ibaraki, 305-0006, Japan.

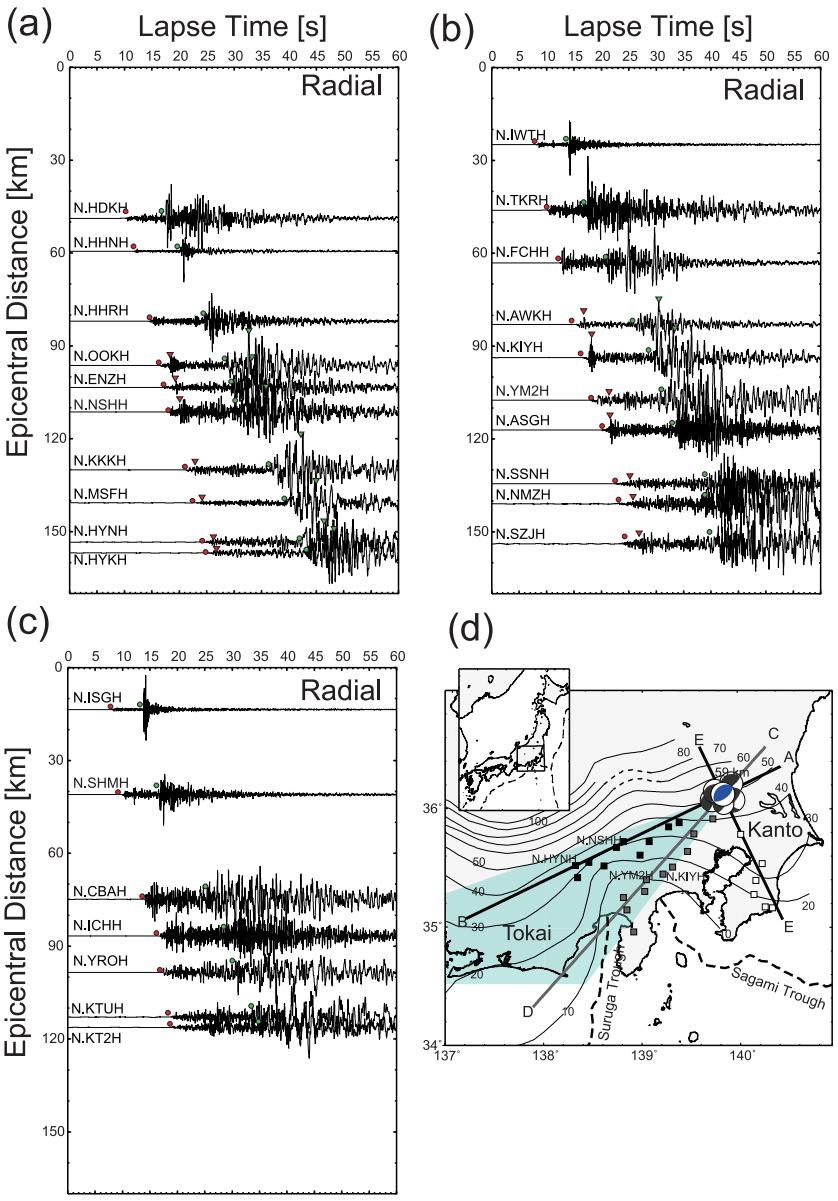


**Figure 1.** Radial-component velocity seismograms observed at Hi-net stations along profiles (a) A–B, (b) C–D and (c) E–F during Event 5 (blue focal sphere). Distribution of seismic stations is shown in (d). Each trace was normalized by its maximum amplitude. Red and green circles represent *P*- and *S*-wave arrivals, respectively. Clear arrivals of trapped *P* and *S* waves are shown by inverse triangles. Isodepth lines of the upper surface of the Philippine Sea plate are shown at 10 km intervals (Baba *et al*. 2002; Hirose *et al*. 2008a,b; Nakajima *et al*. 2009a). Focal depths and mechanisms are from CMT solutions of F-net. The trapped signals can be clearly observed in the light blue area (Hori 1990, 2006).

zone. Propagation features of seismic waves that are trapped or guided through specific structures, such as the crustal layer, fault zones, slabs and seawater, can reflect the structural properties of these structures (e.g. Ben-Zion 1998; Peng *et al*. 2003; Furumura & Kennett 2005; Mizoue & Nishigami 2006; Okal 2008; Obara & Maeda 2009; Lewis & Ben-Zion 2010; Furumura *et al*. 2014). Thus, the characteristics of trapped *P* and *S* waves can be used to reveal various seismic properties of the subducting oceanic crust, such as its geometry, thickness, fluid distribution and the depth of eclogitization (e.g. Fukao *et al*. 1983; Hori 1990; Abers *et al*. 2003; Martin & Rietbrock 2006; Miyoshi *et al*. 2012; Shiina *et al*. 2013). Using observations of trapped waves, Hori (1990) demonstrated that the low-velocity crustal layer of the Philippine Sea plate without eclogitization could be traced to a depth of 60 km beneath the Kanto region in Japan (Fig. 1d). Since this low-velocity layer beneath the Kanto-Tokai region has not been strictly identified as either oceanic or arc crust, we simply refer to this layer as 'subducting crust' in the present study. Recently, Takemura *et al*. (2015b) suggested that the subducting crust of the Philippine Sea plate beneath the Kanto region at depths greater than 40 km is characterized by a uniform velocity layer, and consequently, pulse-like trapped *P* waves are effectively generated around the source regions of earthquakes in the subducting crust. Despite the insight provided by these previous studies, the propagation characteristics of trapped *P* and *S* waves and the internal heterogeneous velocity structure of the subducting crust at shallower depths of less than 40 km have not yet been fully investigated.

In the present study, we analyse velocity seismograms recorded at Hi-net stations around the Kanto region and detect the strong spatial variation in the envelope shapes of trapped *P* and *S* waves.

In order to understand the causes of these variations, we conduct finite difference method (FDM) simulations of seismic wave propagation in both two-dimensional (2-D) and three-dimensional (3-D) models. Following a comparison between observed and simulated seismograms, we demonstrate how the propagation of trapped *P* and *S* waves is affected by the internal heterogeneous velocity structure of the shallower subducting crust of the Philippine Sea plate. Our study may give new insight into the internal heterogeneous velocity structures of the subducting crust and their depth changes in the shallow subducting crust, which may be related to dehydration reactions caused by increasing temperatures and pressures due to subduction.

## 2 CHARACTERISTICS OF OBSERVED TRAPPED WAVES IN THE KANTO REGION

In order to obtain better insight into the lateral variation of observed high-frequency trapped *P* and *S* waves propagating through the subducting crust of the Philippine Sea plate, we analysed waveform data recorded by the dense Hi-net stations around the Kanto-Tokai region, Japan. Hi-net is a high-sensitivity seismograms network operated by the National Research Institute for Earth Science and Disaster Prevention, Japan (Okada *et al*. 2004). Hi-net stations consist of three-component velocity-type seismometers with a natural frequency of 1 Hz, installed at the bottom of boreholes at least 100 m depth.

In the present study, we selected seven earthquakes occurring within the subducting crust of the Philippine Sea plate at depths of 50–60 km beneath the Kanto region (Fig. 1d), based on observations by Hori (1990, 2006) and Takemura *et al*. (2015b). The detailed source parameters of the analysed earthquakes are shown in Table 1. The source mechanisms for each event are referred from the Centroid Moment Tensor (CMT) solutions of F-net (Fukuyama *et al*. 1998; Okada *et al*. 2004).

Fig. 1 shows radial-component velocity seismograms, aligned from the epicentre in different azimuthal directions towards the forearc side, during Event 5. The locations of each profile and of the seismic stations are shown in Fig. 1(d). All seismograms were constructed by correcting the sensor orientation (Shiomi *et al*. 2003) and the frequency response (Maeda *et al*. 2011) of the Hi-net borehole sensors. Trapped *P* and *S* waves could be observed to the southwest of the source (inverse triangles in Figs 1a and b; profiles A–B and C–D), but were less easily identified in the south (Fig. 1c; profile E–F). This azimuthal dependence was consistent among all the events analysed in this study and is also in agreement with the findings of previous studies (Hori 1990, 2006; Takemura & Yoshimoto 2014). Thus, in the present study, we focus our attention on the properties of high-frequency trapped *P* and *S* waves southwest of the earthquake epicentres.

**Table 1.** Source parameters of the earthquakes used in this study.

| No. | Origin time (local time) | Longitude | Latitude | Depth (km) | $M_w$ |
|---|---|---|---|---|---|
| 1 | 2008.04.04 19:01 | 139.828 | 36.120 | 56.0 | 4.8 |
| 2 | 2011.04.02 16:55 | 139.962 | 36.207 | 56.0 | 4.8 |
| 3 | 2011.04.26 21:12 | 139.976 | 36.086 | 59.0 | 4.9 |
| 4 | 2012.02.11 10:26 | 139.789 | 36.088 | 59.0 | 4.8 |
| 5 | 2012.05.18 17:18 | 139.841 | 36.136 | 59.0 | 4.8 |
| 6 | 2012.07.16 04:31 | 139.817 | 36.152 | 62.0 | 4.8 |
| 7 | 2013.02.01 01:04 | 139.893 | 36.056 | 50.0 | 4.3 |

Fig. 2 shows the vertical and transverse component seismograms along profiles A–B and C–D to which reduction velocities of 8.0 and 4.5 km $s^{-1}$ were applied, respectively. It was found that, along profile A–B (Fig. 2a), very clear pulse-like trapped waves propagated over wide epicentral distances (80–150 km), although the amplitudes of the trapped waves decayed suddenly at distances greater than 140 km. In contrast, along profile C–D (Fig. 2b), the observations of pulse-like trapped waves were limited to epicentral distances of 80–100 km. At distances greater than 100 km, the trapped waves seem to be smeared out.

The lateral variation in the trapped waves described above represents a single set of observations from Event 5. Therefore, a stochastic quantitative analysis should be applied to all the seismograms from the other studied events. Based on the method proposed by Takemura *et al*. (2015b), the root mean square (RMS) envelopes of *P* and *S* waves at each station for different frequencies of 1–2, 2–4, 4–8 and 8–16 Hz were calculated by the sum of the three-component envelopes of filtered seismograms. The amplitudes of the RMS envelopes for *P* and *S* waves were normalized by the maximum amplitude in a 15 s time window, starting 5 s prior to the arrivals of the *P* and *S* waves, respectively. Fig. 3 shows filtered full-length, zoom-in three-component seismograms and RMS envelopes for trapped *P* and *S* waves recorded at the N.NSHH station during Event 5. By stacking the normalized RMS envelopes of all earthquakes at each station, we obtained averaged RMS envelopes for the *P* and *S* waves that reflect the average path effects from source to receiver.

Fig. 4 shows the typical stacked RMS envelopes of trapped *P* and *S* waves for each frequency band at four Hi-net stations along two southwest profiles. The trapped *P* and *S* waves were observed clearly at stations along profile A–B (N.NSHH and N.HYNH; Fig. 4a), showing pulse-like envelopes without significant dispersion and peak delays. The averaged amplitudes of the trapped *P* and *S* waves were 5–7 and 3–4 times larger than those of the *P* and *S* waves, respectively. These features were consistent, irrespective of frequency.

Along the profile C–D, the stacked RMS envelopes of trapped *P* and *S* waves were also pulse-like at N.KIYH (left side of Fig. 4b). However at the relatively distant station of N.YM2H, located 108 km from the epicentre, the envelopes exhibited gradual increases in amplitude with strong peak delay and became characteristically 'spindle-shape'. This confirms the qualitative observations of the lateral variation of trapped waves along the profile C–D in Fig. 2. At distant stations, although trapped wave energy appears just 2–3 s after the arrival of the weak body waves, the envelopes of the trapped *P* and *S* waves were not pulse-like shape but spindle shape with a strong peak delay and pulse broadening.

## 3 2-D SIMULATION OF SEISMIC WAVE PROPAGATION: EFFECTS OF SEISMIC WAVE SCATTERING IN SUBDUCTING CRUST

### 3.1 Method and model for 2-D simulations

We suggest that the observations reported in the preceding section may be caused by lateral variations in the heterogeneous structure of the subducting crust of the Philippine Sea plate, especially at shallower depths. To verify this, we simulate seismic wave propagation in realistic velocity structure models to model the observed trapped *P* and *S* waves. As the first stage of our study, we conducted 2-D FDM simulations and discuss the differences between both

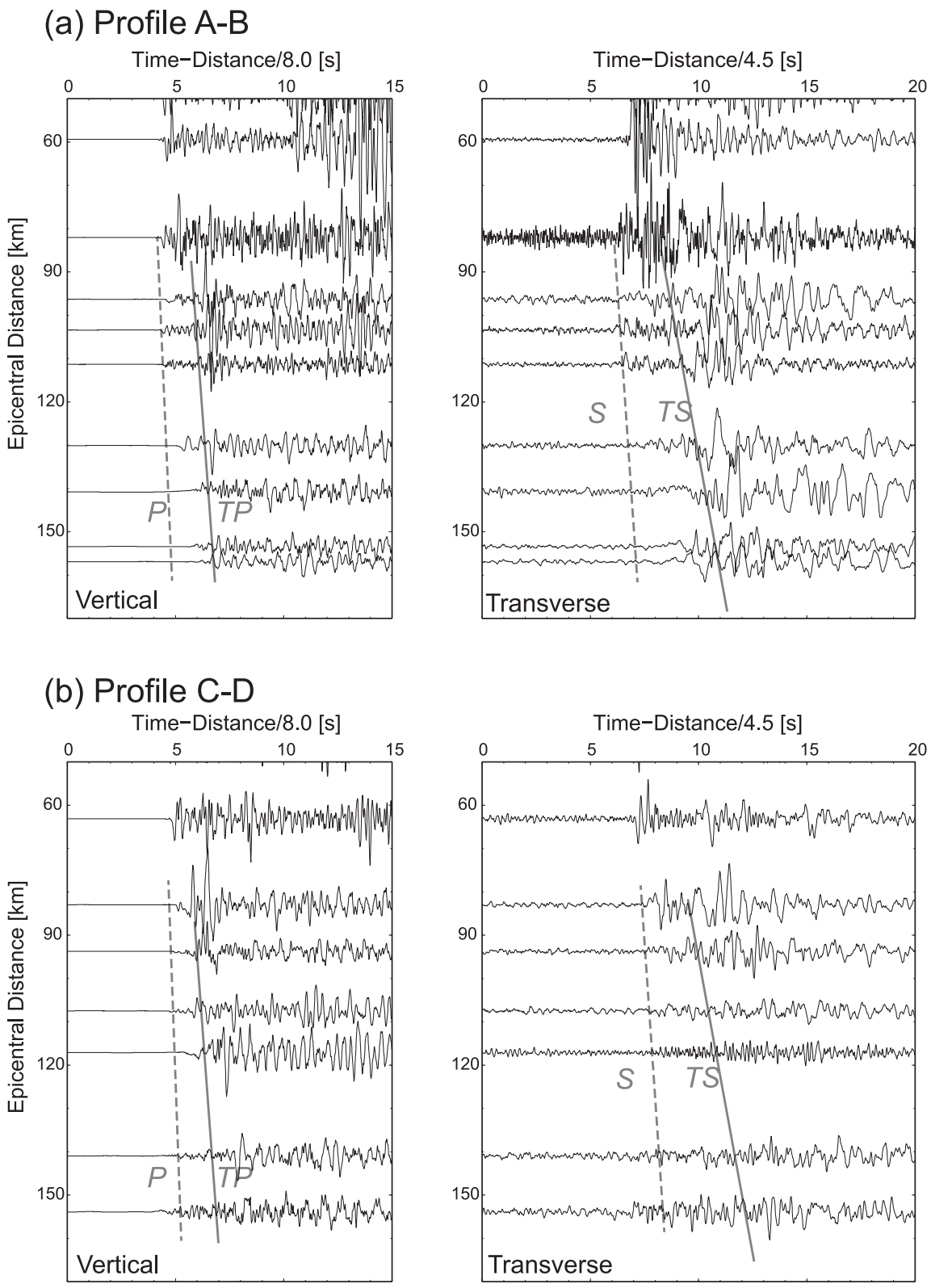


**Figure 2.** Vertical and transverse seismograms observed at Hi-net stations along profiles (a) A–B and (b) C–D during Event 5. Reduction velocities for vertical and transverse components are 8.0 and 4.5 km $s^{-1}$, respectively. To magnify small amplitudes observed at distant stations, the amplitudes of each trace were multiplied by their epicentral distance.

profiles using various heterogeneous models. 3-D simulations were then conducted to verify the results of the 2-D simulations and to discuss the lateral variations in the propagation of trapped waves within a 3-D heterogeneous structure.

The 2-D simulation model covered an area of $327.68 \times 102.4$ $km^2$ in the horizontal and vertical directions, respectively. To achieve a precise simulation of the seismic *P–SV* wavefield for frequencies up to 16 Hz, the model was discretized by a grid interval of

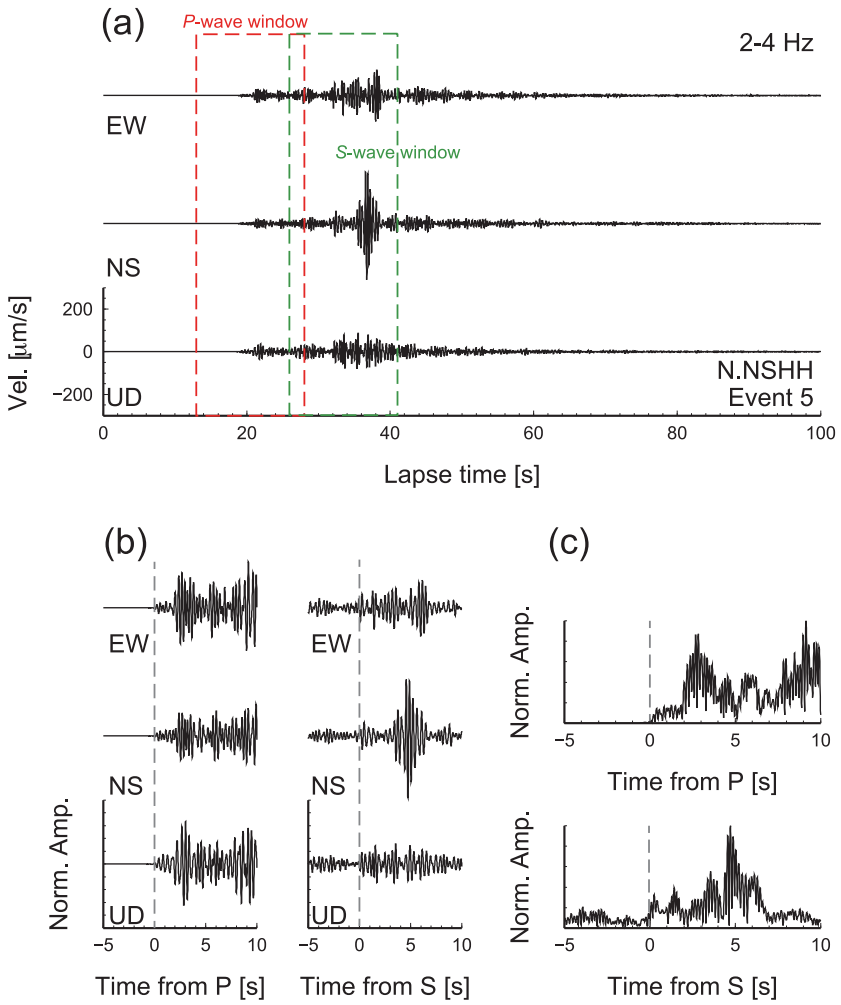


**Figure 3.** (a) Three-component velocity seismograms for frequency of 2–4 Hz, (b) normalized filtered seismograms and (c) RMS envelopes for trapped *P* and *S* waves at N.NSHH during Event 5. Time windows for trapped *P* and *S* waves are represented by red and green dashed rectangles, respectively.

0.02 km, and a domain partitioning technique using the Message Passing Interface was employed (e.g. Furumura & Chen 2004; Maeda & Furumura 2013; Takemura *et al*. 2015a). Other technical details are the same as the described by Takemura *et al*. (2015a,b).

The background velocity structure was constructed using the Japan Integrated Velocity Structure Model (JIVSM) proposed by Koketsu et al. (2008, 2012), which includes a two-layered low-velocity crustal structure at the top of the Philippine Sea plate. Referring to Takemura *et al*. (2015b) for the modelling of trapped waves, we assumed a uniform velocity crust of the Philippine Sea plate at depths greater than 40 km. We also introduced a low-velocity anomaly into the simulation model, in which the seismic *P*- and *S*-wave velocities were reduced by 10 per cent compared with the original JIVSM. This low-velocity anomaly (blue triangles in Figs 5 and 7), which was originally detected by tomography studies (e.g. Matsubara *et al*. 2005), is located in the lower crust and the mantle in the JIVSM. The thickness of the Philippine Sea plate was assumed to be approximately 50 km (e.g. Kumar & Kawakatsu 2011; Tonegawa & Helffrich 2012). We did not include the low-velocity ($V_S < 3$ km s$^{-1}$) sedimentary Kanto Basin in the model.

We employed a frequency-dependent intrinsic attenuation ($Q_{\rm Int}{}^{-1}$) model for *P* and *S* waves, based on the method of Robertsson (1994). We adopt a single relaxation mechanism with a reference frequency of $f_0 = 2$ Hz, which gives a peak $Q_{\rm Int}{}^{-1}$ value at this frequency referred from JIVSM.

A double-couple point source was set at a depth of 50 km (stars in Figs 5 and 7). The normalized source time function was represented by a single-cycle Kupper wavelet with $T_0 = 0.16$ s (e.g. Mavroeidis & Papageorgiou 2003). Source depth was modified from the original CMT solution (59 km) in order to set the source within the subducting crust of the assumed velocity structure model, since large amplitude trapped seismic waves are not observed for earthquakes occurring outside this layer (e.g. Miyoshi *et al*. 2012).

Takemura *et al*. (2015b) confirmed that the trapped waves that develop in the subducting crust preserve their amplitudes during propagation through the crust and mantle with small-scale heterogeneities. Thus, the observed spindle-shape envelopes may be caused by scattering due to strong small-scale velocity heterogeneities in the subducting crust. To model small-scale velocity heterogeneities, stochastic random velocity fluctuation $\xi(\boldsymbol{x})$ characterized by a von Kármán or Gaussian power spectral density function (PSDF) was embedded over an average background velocity $V_0(\boldsymbol{x})$ (e.g. Frankel & Clayton 1986; Sato *et al*. 2012), which is described as $V(\boldsymbol{x}) = V_0(\boldsymbol{x})[1+\xi(\boldsymbol{x})]$. The observed envelopes of trapped waves along the profile C–D were characterized by spindle shape irrespective of frequency. Recently, Takemura & Yoshimoto (2014)

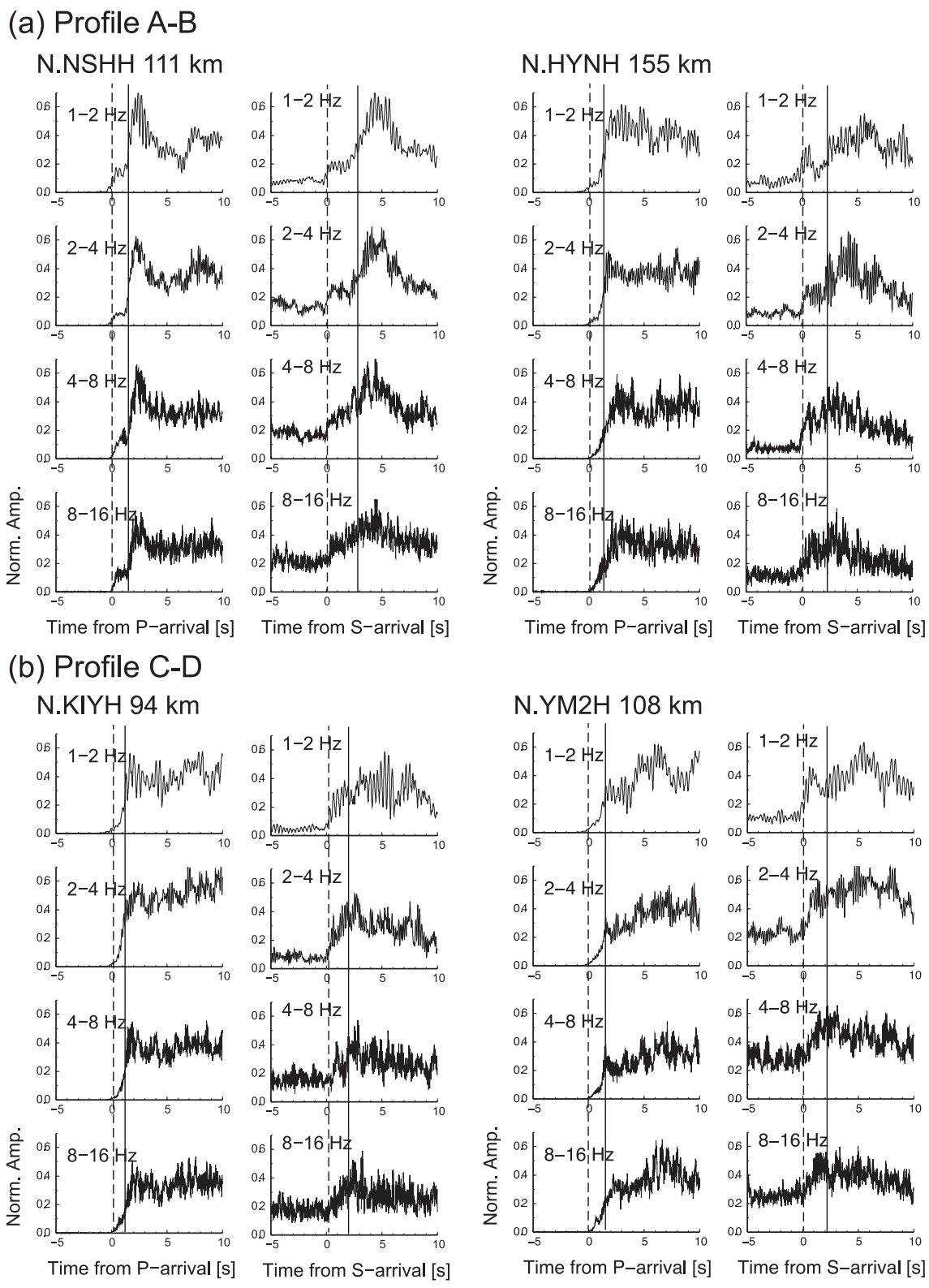


**Figure 4.** Normalized RMS envelopes of trapped *P* and *S* waves for different frequency bands along profiles (a) A–B and (b) C–D. Time was measured from the arrivals of the *P* and *S* waves. The average epicentral distances of stations N.NSHH, N.HYNH, N.KIYH and N.YM2H are 111, 155, 94 and 108 km, respectively. The locations of the stations are shown in Fig. 1(d).

demonstrated that frequency-independent spindle-shape seismograms with strong peak delays could be successively reproduced by introducing a specific heterogeneity model into the low-velocity anomaly of the lower crust and subducting crust of the Philippine Sea plate. This heterogeneity model is characterized by a Gaussian PSDF (correlation distance of $a = 1$ km, RMS value of $\varepsilon = 0.07$) superposed on a background exponential PSDF ($a = 3$ km, $\varepsilon = 0.07$). As such, we incorporated this model into the subducting

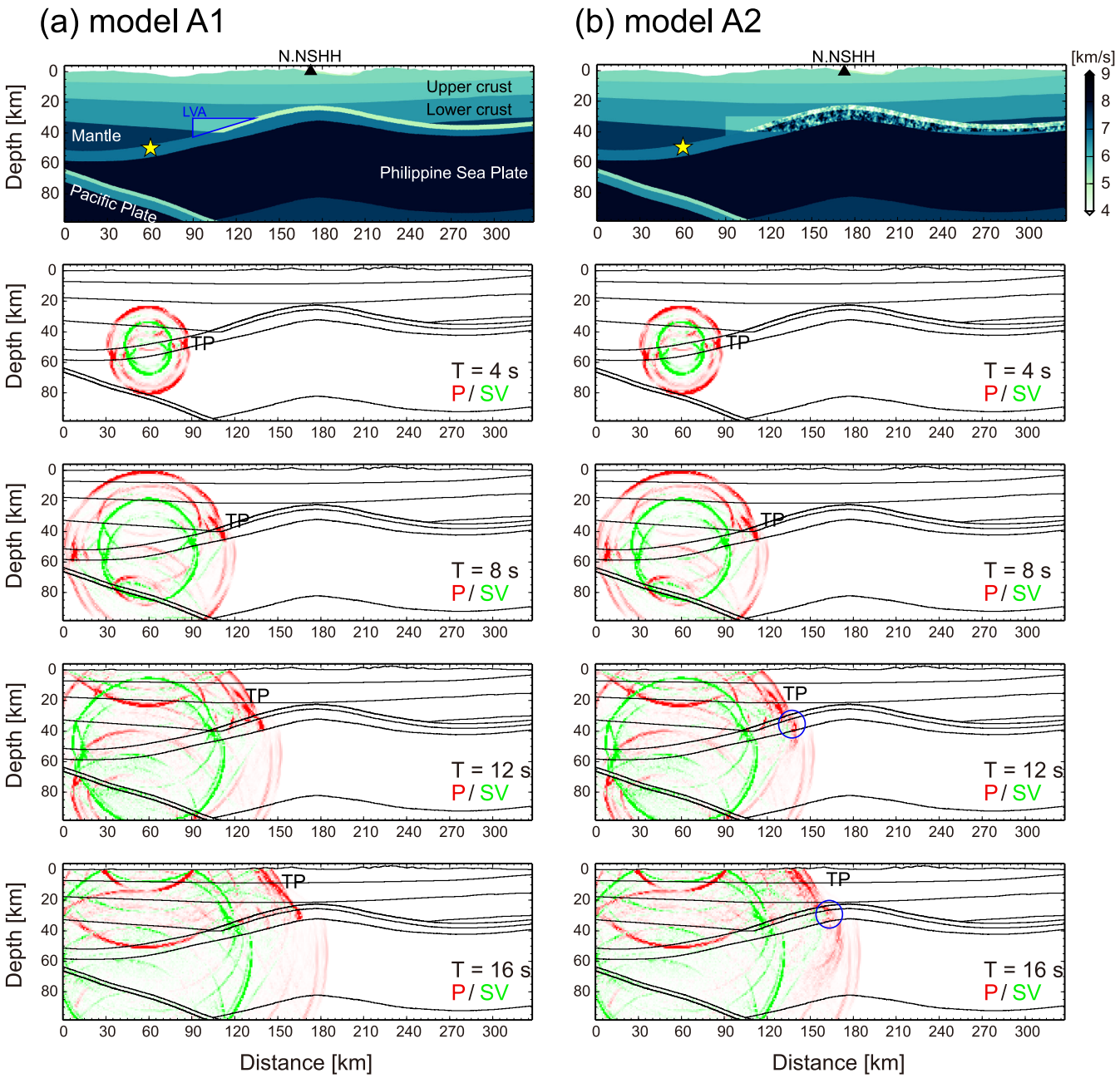


**Figure 5.** Snapshots of the seismic wave propagation at lapse times of $t = 4$, 8, 12 and 16 s, derived from 2-D FDM simulations in (a) model A1 and (b) model A2 along profile A–B. Assumed *P*-wave velocity structures are shown in the upper panels. The yellow star marks the location of the hypocentre. The 2-D *P* (red) and *SV* (green) wavefields were evaluated by their divergence and rotation, respectively.

**Table 2.** Parameters of small-scale velocity heterogeneities in each model.

| | Crustal layer of the Philippine Sea plate | Crust, mantle and oceanic mantle |
|---|---|---|
| Model A1 | – | – |
| Model A2 | Gaussian ($a = 1$ km, $\varepsilon = 0.07$) + exponential ($a = 3$ km, $\varepsilon = 0.07$) | – |
| Model A3 | Gaussian ($a = 1$ km, $\varepsilon = 0.07$) + exponential ($a = 3$ km, $\varepsilon = 0.07$) | Table 4 of Takemura & Yoshimoto (2014) |

crust at depths of less than 40 km. The parameters of the small-scale velocity heterogeneities in each model are shown in Table 2.

The *P*-wave velocity structure models used in our simulations are shown in the upper panels of Figs 5 and 7. Model A1 (upper panels of Figs 5a and 7a) is a simple layered structure model and is used as a reference. The more realistic model A2 was constructed to incorporate small-scale velocity heterogeneities in the subducting crust at depths less than 40 km (top panels of Figs 5b and 7b).

### 3.2 Results of 2-D simulations

Figs 5 and 6 illustrate snapshot sequences of seismic wave propagation and synthetic waveforms of the vertical component along profile A–B. The 2-D *P* (red) and *SV* (green) wavefields were evaluated in terms of their divergence and rotation, respectively.

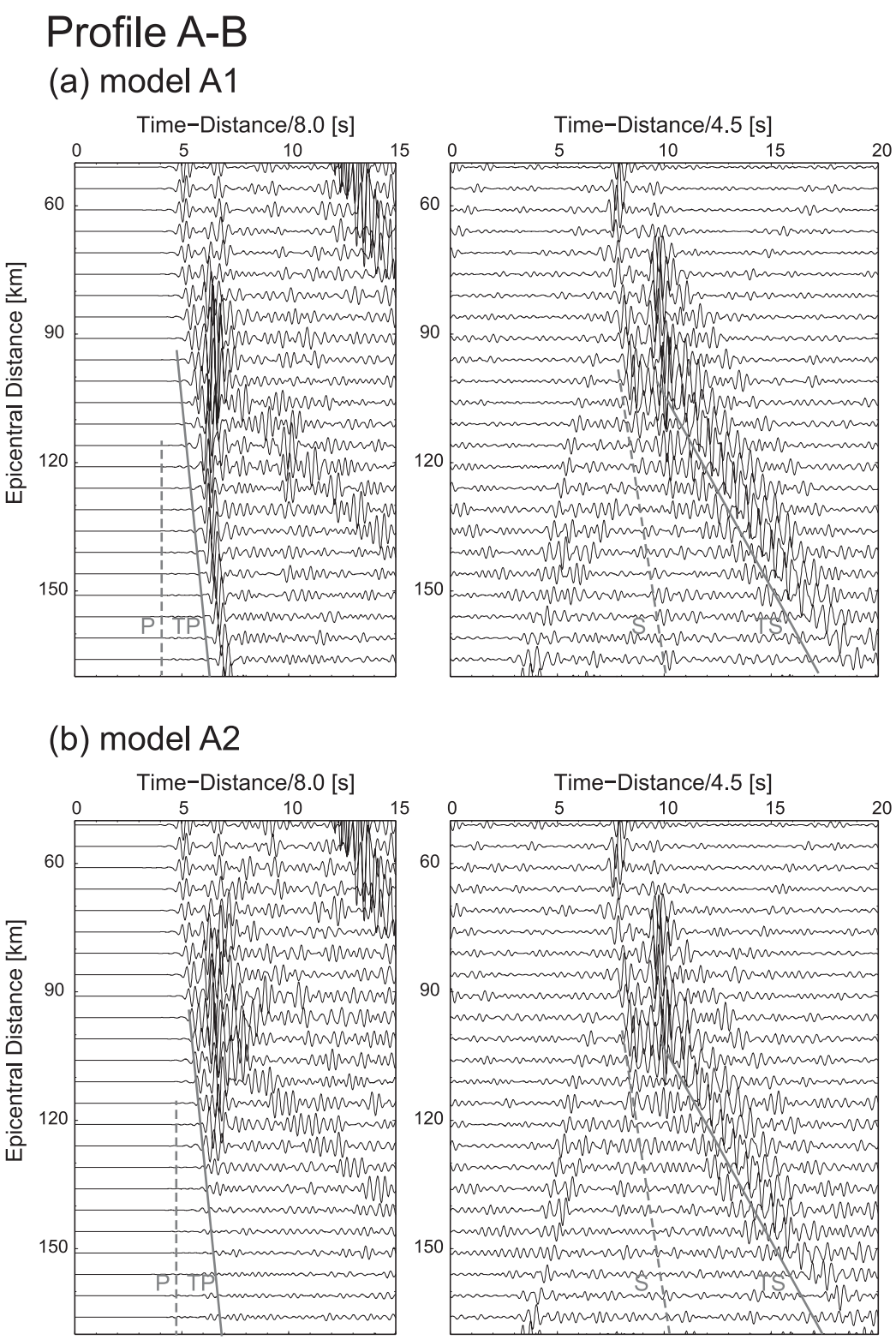


**Figure 6.** Vertical component seismograms for frequency of 2–4 Hz derived from the 2-D simulations of (a) model A1 and (b) model A2 along profile A–B. Grey solid and dashed lines indicate the arrivals of the trapped and direct body waves, respectively. Reduction velocities for *P* and *S* waves are 8.0 and 4.5 km $s^{-1}$, respectively. To magnify small amplitudes observed at distant stations, the amplitudes of each trace were multiplied by root of their epicentral distance.

At an early lapse time of $T = 4$ s, distinct trapped *P* waves (marked TP in Fig. 5) were generated around the source region and then propagated along the low-velocity subducting crust. Trapped energy was released into the crust at depths of 35 km, and could be observed as pulse-like trapped *P* waves at shorter epicentral distances (Fig. 6). The unreleased trapped energy in the subducting crust could still propagate effectively in model A1, whereas in model A2 it scattered by seismic wave scattering due to the small-scale velocity

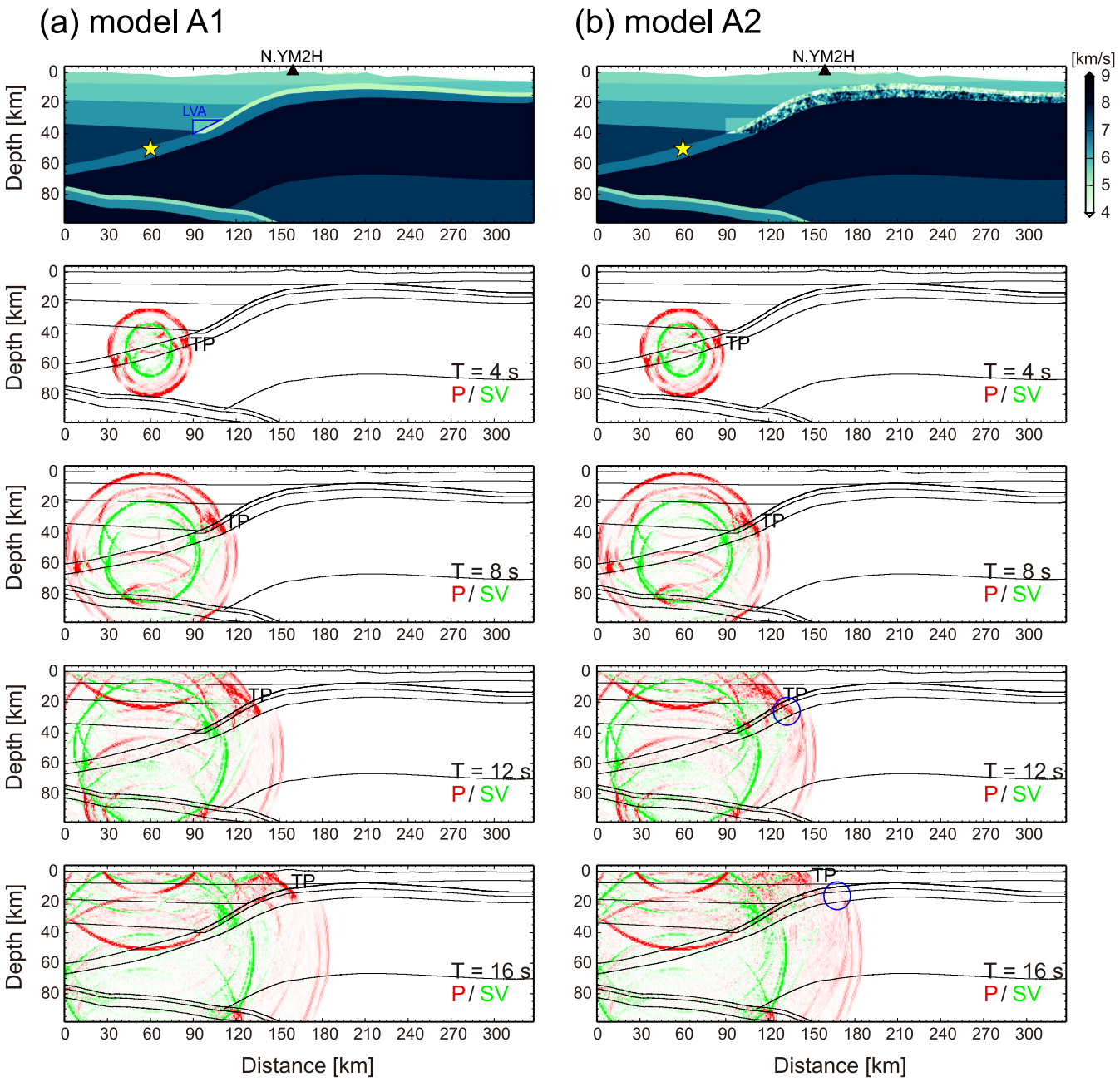


**Figure 7.** Snapshots of the seismic wave propagation at lapse times of $t$ = 4, 8, 12 and 16 s, derived from 2-D FDM simulations in (a) model A1 and (b) model A2 along profile C–D. Assumed *P*-wave velocity structures are shown in the upper panel. The yellow star marks the location of the hypocentre. The 2-D *P* (red) and *SV* (green) wavefields were evaluated by their divergence and rotation, respectively.

heterogeneities in the shallower subducting crust (blue circle in Fig. 5b). From these simulation results, it can be seen that the trapped *P* waves predicted by model A1 are inconsistently strong compared with the observations at epicentral distances of around 150 km (Fig. 2).

Since the subducting crust along profile C–D is up dip and subparallel to the shortest ray path between the source and receivers at epicentral distances of around 100 km (Fig. 1d and upper panels of Fig. 7), trapped *P* waves propagated mainly through the subducting crust. In model A1 (Figs 7a and 8a), distinct trapped waves without peak delay and dispersion could propagate even greater distances. However, in model A2, the trapped energy was significantly decreased because of the scattering due to small-scale velocity heterogeneities in the shallower (<40 km) subducting crust. Sudden decreases in the amplitudes of trapped waves were found in the synthetic seismograms from model A2 at distances of around 100 km. At greater distances, the arrivals of trapped waves became unclear and the pulse-like envelope shapes were not preserved.

To confirm the effects of crustal scattering on the trapped waves, we conducted additional FDM simulations using model A3 (lower panels in Fig. 9), which is similar to model A2, but with small-scale velocity heterogeneities in the crust, mantle and oceanic mantle (Table 2). We assumed an exponential PSDF to represent heterogeneities in the crust, mantle and oceanic mantle, and the parameters of the PSDFs were provided by previous studies (e.g.

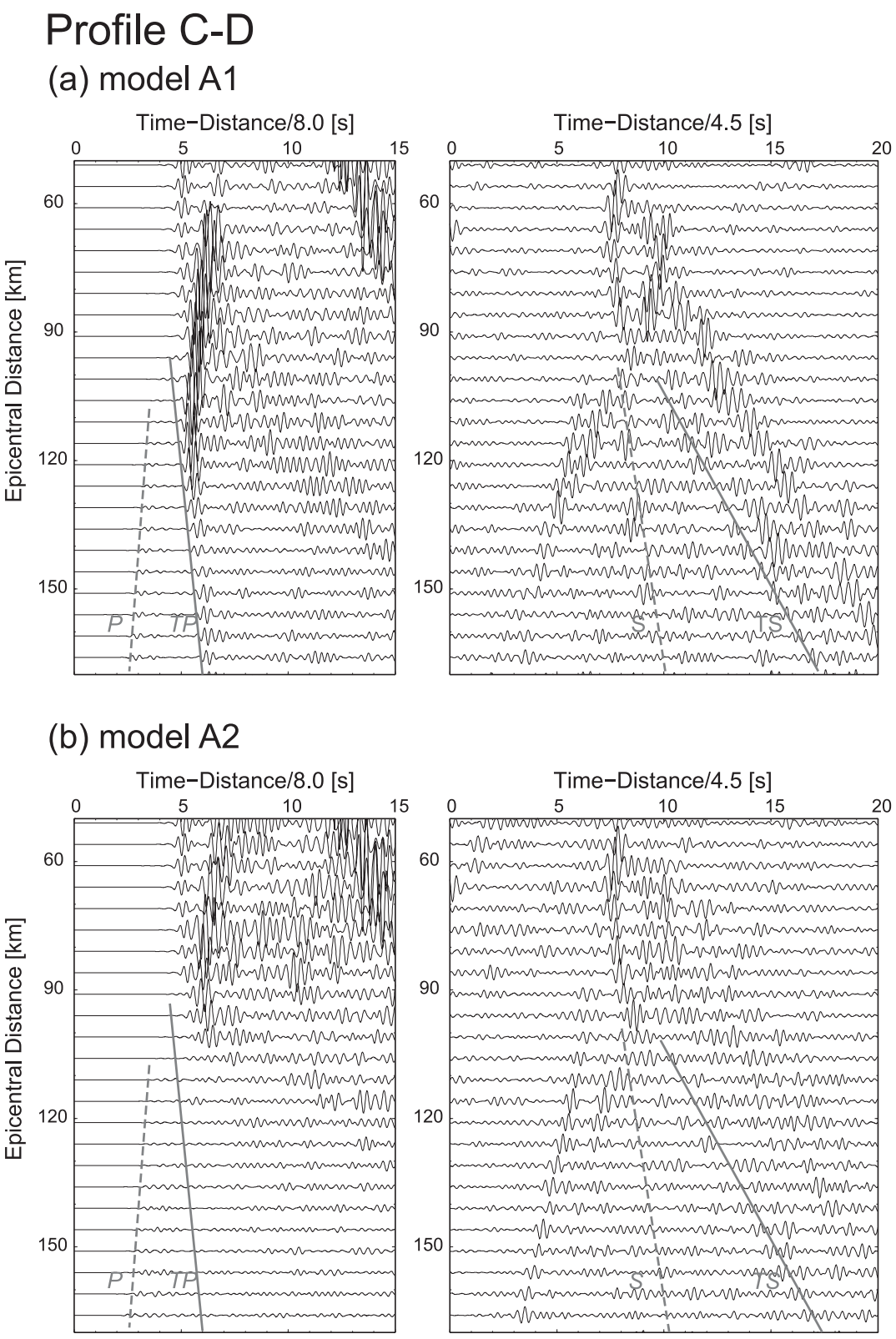


**Figure 8.** Vertical component seismograms for frequency of 2–4 Hz derived from the 2-D simulations of (a) model A1 and (b) model A2 along profile C–D. Grey solid and dashed lines indicate the arrivals of trapped and direct body waves, respectively. The reduction velocities for *P* and *S* waves are 8.0 and 4.5 km $s^{-1}$, respectively. To magnify small amplitudes observed at distant stations, the amplitudes of each trace were multiplied by root of their epicentral distance.

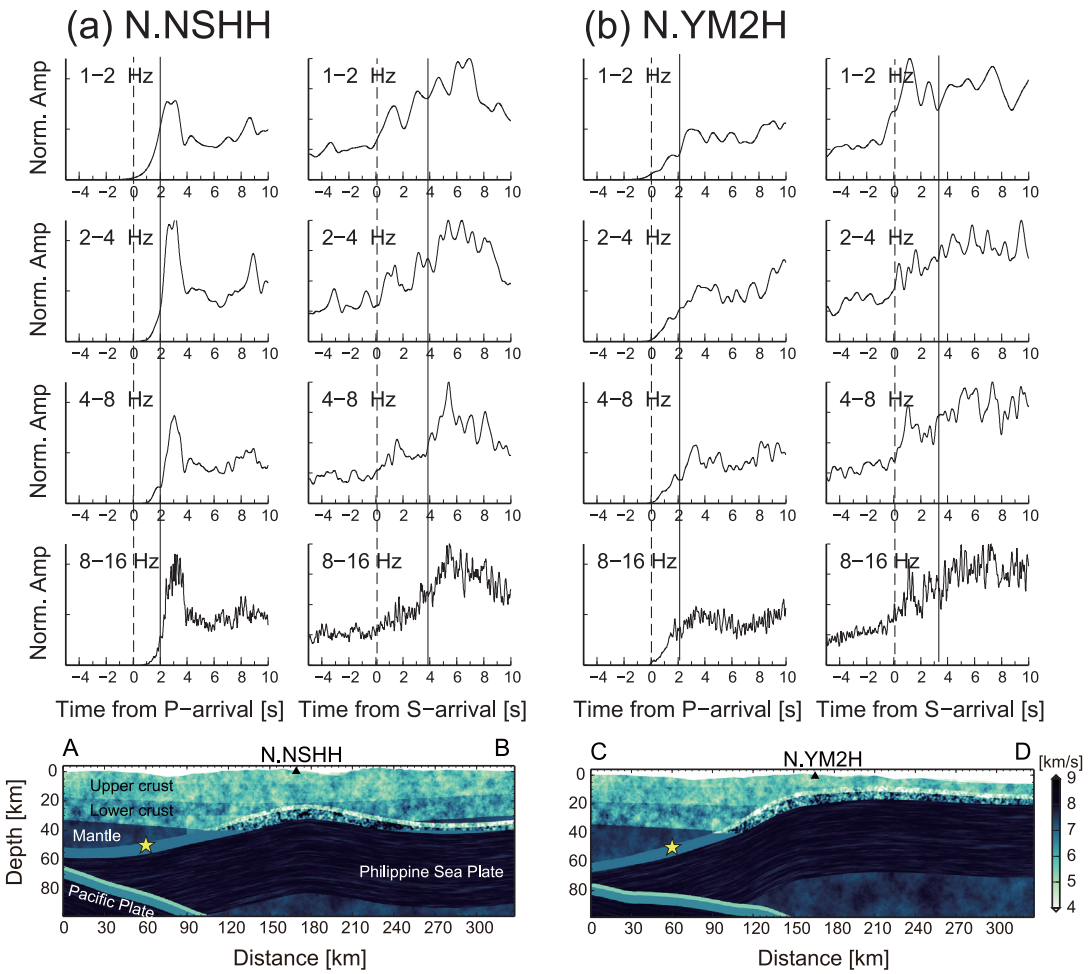


**Figure 9.** Simulated RMS envelopes at stations (a) N.NSHH and (b) N.YM2H for different frequency bands, derived from 2-D simulations using model A3. Assumed *P*-wave velocity structure models are shown in the lower panels.

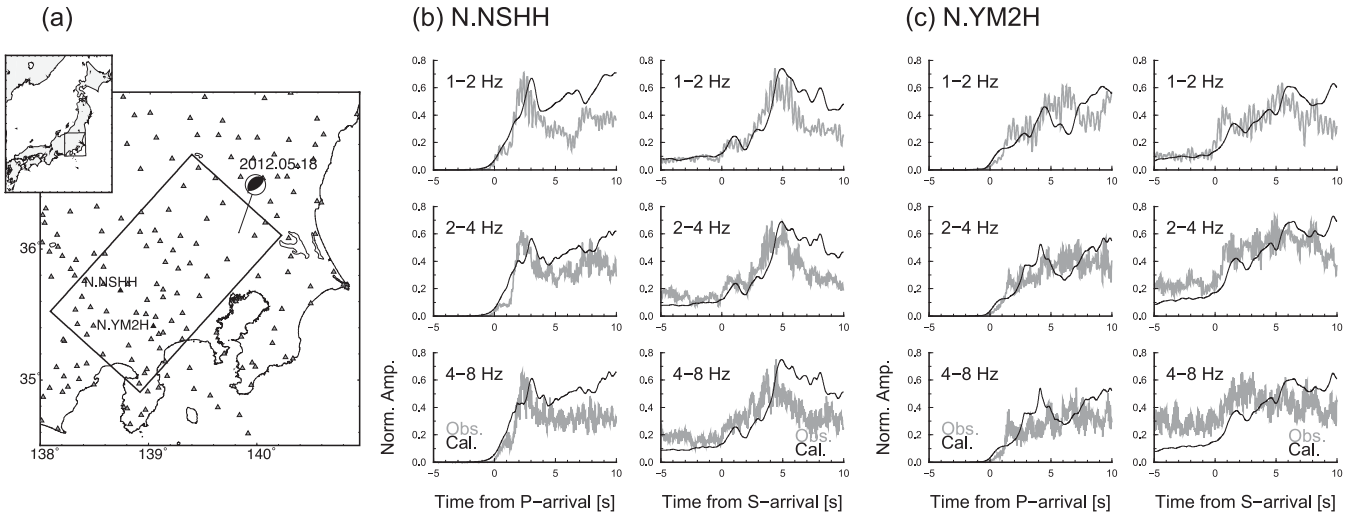


**Figure 10.** Comparison between observed and 3-D-simulated RMS envelopes for trapped *P* and *S* waves. (a) Area of 3-D simulation, (b) RMS envelopes at N.NSHH and (c) RMS envelopes at N.YM2H. Solid rectangle shows the horizontal area of the 3-D simulation. Black and grey lines show the simulated and observed RMS envelopes, respectively.

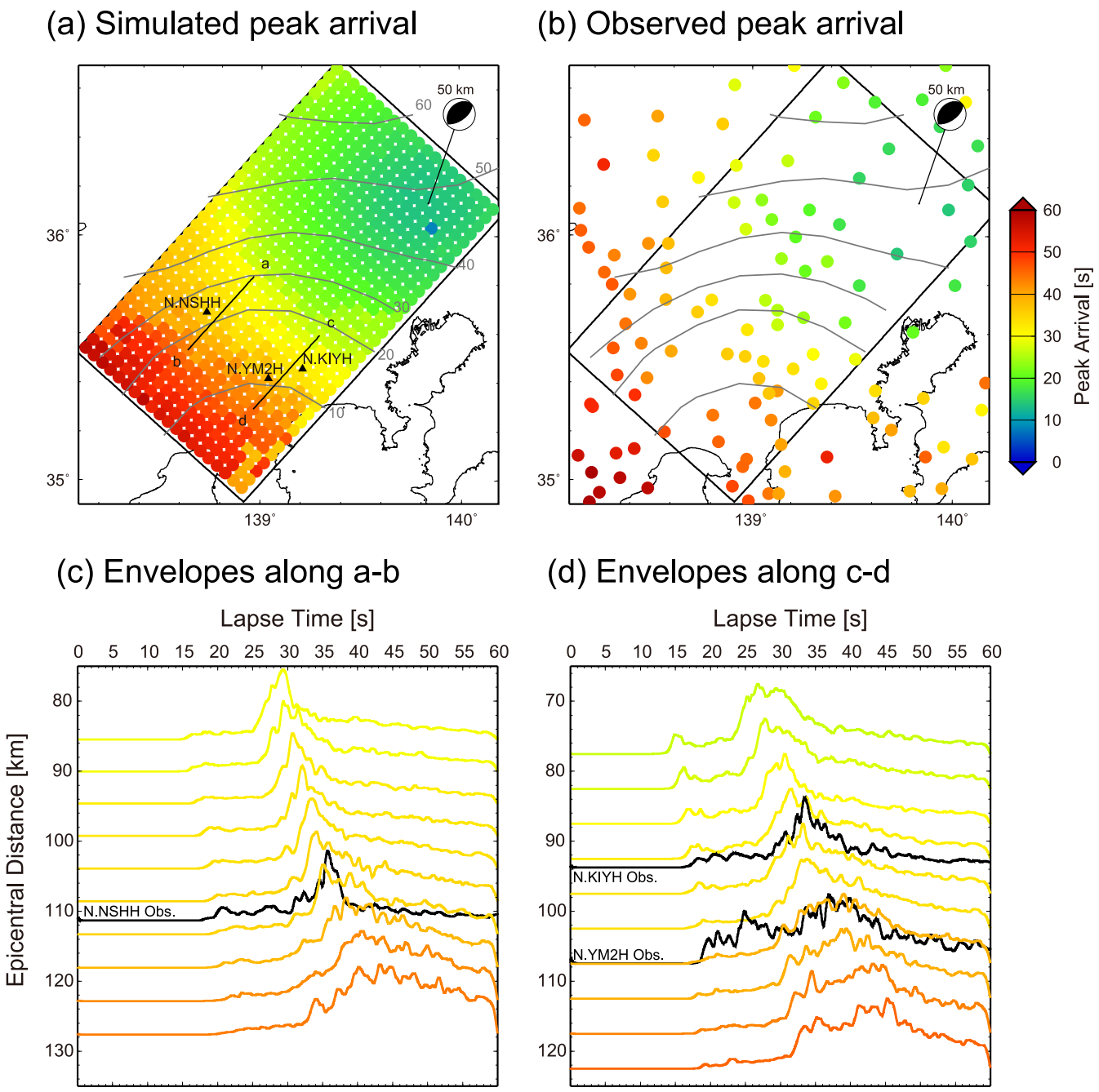


**Figure 11.** Spatial distributions of peak arrival times from (a) simulations and (b) observations. RMS envelopes along profiles (c) A–B and (d) C–D derived from observations and simulations. A bandpass filter with frequency of 2–4 Hz was applied to each trace. The amplitudes of envelopes were normalized by their maximum amplitudes.

Furumura & Kennett 2005; Takemura *et al*. 2009; Takemura & Furumura 2013). Detailed parameters are summarized in table 4 of Takemura & Yoshimoto (2014).

Fig. 9 shows the normalized RMS envelopes of trapped *P* and *S* waves at N.SNHH and N.YM2H for different frequency bands. The RMS envelopes were calculated as ensemble averages of ten realizations of stochastic velocity heterogeneities. Despite the introduction of small-scale velocity heterogeneities into the crust, mantle and oceanic mantle, the dominant features of the trapped waves along both profiles were preserved and agreed well with the observations.

## 4 PROPAGATION OF TRAPPED WAVES IN A 3-D HETEROGENEOUS STRUCTURE INFERRED FROM 3-D SIMULATION

In the previous sections, we demonstrated that the observed characteristics of trapped *P* and *S* waves could be reproduced by 2-D FDM simulations. As the next step, we conducted a 3-D FDM simulation of Event 5 to directly compare the simulation results with observed waveforms and to discuss the propagation and scattering of trapped waves in a realistic 3-D heterogeneous structure model.

The model used in the 3-D simulation covered an area of 153.6 × 76.8 × 75.0 km$^3$ in the horizontal and vertical directions (solid rectangle in Fig. 10a) and was discretized by a grid interval of 0.05 km. The 3-D velocity structure was assumed to be the same as in the previous simulations (model A3; Fig. 9). Based on the minimum *S*-wave velocity and grid spacing, our 3-D simulation was able to examine seismic wave propagation for frequencies below 8 Hz with a sampling of eight grid points per minimum *S* wavelength. Takemura *et al*. (2015a) demonstrated that FDM simulations under these calculation conditions were sufficient to discuss the scattering of high-frequency seismic waves, even if the model includes both topographic variations and small-scale velocity heterogeneities. The present large-scale FDM simulations were conducted on the Earth Simulator (ES2) at the Japan Agency for Marine-Earth Science and Technology (JAMSTEC), requiring a computer memory of 2.3 TB and a wall-clock time of 4.1 h by parallel computing using 60 nodes (480 CPUs) of the ES2, to evaluate seismic wave propagation for 60 s by 24 000 time-step calculations.

In the 3-D simulations, we employed a source time function represented by an asymmetric cosine function (Ji *et al*. 2003) with $M_0 = 2.11 \times 10^{16}$ Nm, $t_s = 0.15$ and $t_e = 0.35$ s. This function is more realistic compared with the single-cycle Kupper wavelet employed in the 2-D simulation, as two time parameters control the rise time and the duration of the source rupture. The two time parameters, $t_s$ and $t_e$, were determined from displacement waveforms at the F-net station nearest the epicentre. The seismic moment $M_0$ was obtained from the F-net CMT solution of Event 5.

Fig. 10 shows a comparison of observed and 3-D simulated trapped *P*- and *S*-wave envelopes at N.NSHH and N.YM2H. Simulated RMS envelopes (black lines in Figs 10b and c) were calculated from the ensemble averages of vector RMS envelopes from ten realizations of stochastic random velocity heterogeneities. The amplitudes of simulated RMS envelopes were normalized by the maximum amplitudes of observed envelopes for each time window, in order to focus on the envelope shapes and relative amplitudes of the direct and trapped waves. The simulation results well reproduce the observed characteristics of trapped *P* and *S* waves at both stations, including the frequency-independent envelope shape and the amplitude ratio between direct and trapped signals. This indicates that the model discussed in the previous section is valid not only in 2-D space, but also in 3-D space.

To investigate the characteristics of seismic wave propagation in a 3-D heterogeneous structure, we examined the spatial variations of peak arrival times and envelope shapes at dense virtual stations with a uniform interval of 5 km. Fig. 11 is a comparative plot of the spatial variation in peak arrival times and RMS envelopes for frequency of 2–4 Hz, derived from the 3-D FDM simulations and the observations by Hi-net. RMS envelopes from the 3-D FDM simulation are coloured to show the peak arrival times of each envelope, while the observed RMS envelopes at each Hi-net station during Event 5 are marked in black.

The peak arrival times in the 3-D heterogeneous model (Fig. 11a) did not show a simple symmetric concentric pattern around the epicentre. Strong delays in peak arrival times were detected in those regions where the Philippine Sea plate exists at shallow depths of less than 15 km. This pattern was also identified in the observed peak arrival times (Fig. 11b). The simulated RMS envelopes also showed good agreement with the observed spatial variation in envelope shapes (Figs 11c and d). As shown in the snapshots of the 2-D simulations (Fig. 7b), simulated RMS envelopes at distances greater than 105 km along profile C–D were significantly distorted by seismic wave scattering due to small-scale velocity heterogeneities in the shallower subducting crust. Thus, the configuration of the subducting Philippine Sea plate and scattering in the shallower subducting crust can be seen to strongly affect the seismogram envelopes during intraslab earthquakes beneath the Kanto region.

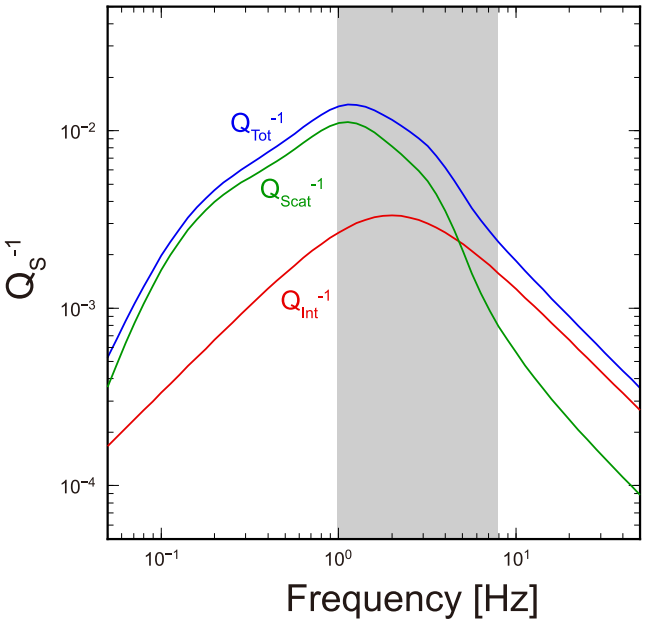


**Figure 12.** Assumed $Q$ model in the subducting crust. Blue, green and red lines show the total, scattering and intrinsic attenuations for *S* waves, respectively. The grey shaded area represents the frequency range of our observations and simulations.

We evaluated the scattering attenuation $Q_{Scat}^{-1}$ for *S* waves, based on the first-order Born approximation (Sato 1984), assuming strong velocity heterogeneities given by the superposition of an exponential PSDF with $a = 3$ km, $\varepsilon = 0.07$ and a Gaussian PSDF with $a = 1$ km, $\varepsilon = 0.07$. Fig. 12 shows the scattering attenuation $Q_{Scat}^{-1}$, the assumed intrinsic attenuation $Q_{Int}^{-1}$ and the total attenuation $Q_{Tot}^{-1}$, in the subducting crust from our simulations, assuming *P*- and *S*-wave velocities of 6.8 and 4.0 km s$^{-1}$. The assumed intrinsic attenuation $Q_{Int}^{-1}$ is same as in model A3, in which a single relaxation mechanism with a reference frequency of $f_0 = 2$ Hz and peak values of $Q_0^{-1} = 1/300$ is assumed. The total attenuation $Q_{Tot}^{-1}$ for *S* waves is estimated as $Q_{Int}^{-1} + Q_{Scat}^{-1}$.

Estimated values of $Q_{Scat}^{-1}$ for frequencies lower than 4 Hz are much larger than those of $Q_{Int}^{-1}$, implying that scattering attenuation is the dominant mechanism of seismic attenuation in the shallower subducting crust at these frequencies. The estimated total attenuation $Q_{Tot}^{-1}$ agrees with that found in previous studies of tremor amplitudes attenuation in the subducting oceanic crust of the Philippine Sea plate around the Nankai subduction zone (Yabe *et al*. 2014). At depths greater than 40 km, small-scale velocity heterogeneities in the subducting crust disappear, and consequently attenuation is expected to weaken because the seismic wave scattering becomes less dominant. This also agrees well with the results of $Q$ tomography by Takaoka *et al*. (2012), who noted that the $Q$ value in the oceanic crust beneath the Kii Peninsula increases at depths greater than around 40 km.

## 5 DISCUSSIONS AND CONCLUSION

In the Kanto region, analysis of Hi-net waveform data from earthquakes occurring in the subducting crust of the Philippine Sea plate revealed strong lateral variation in the characteristics of

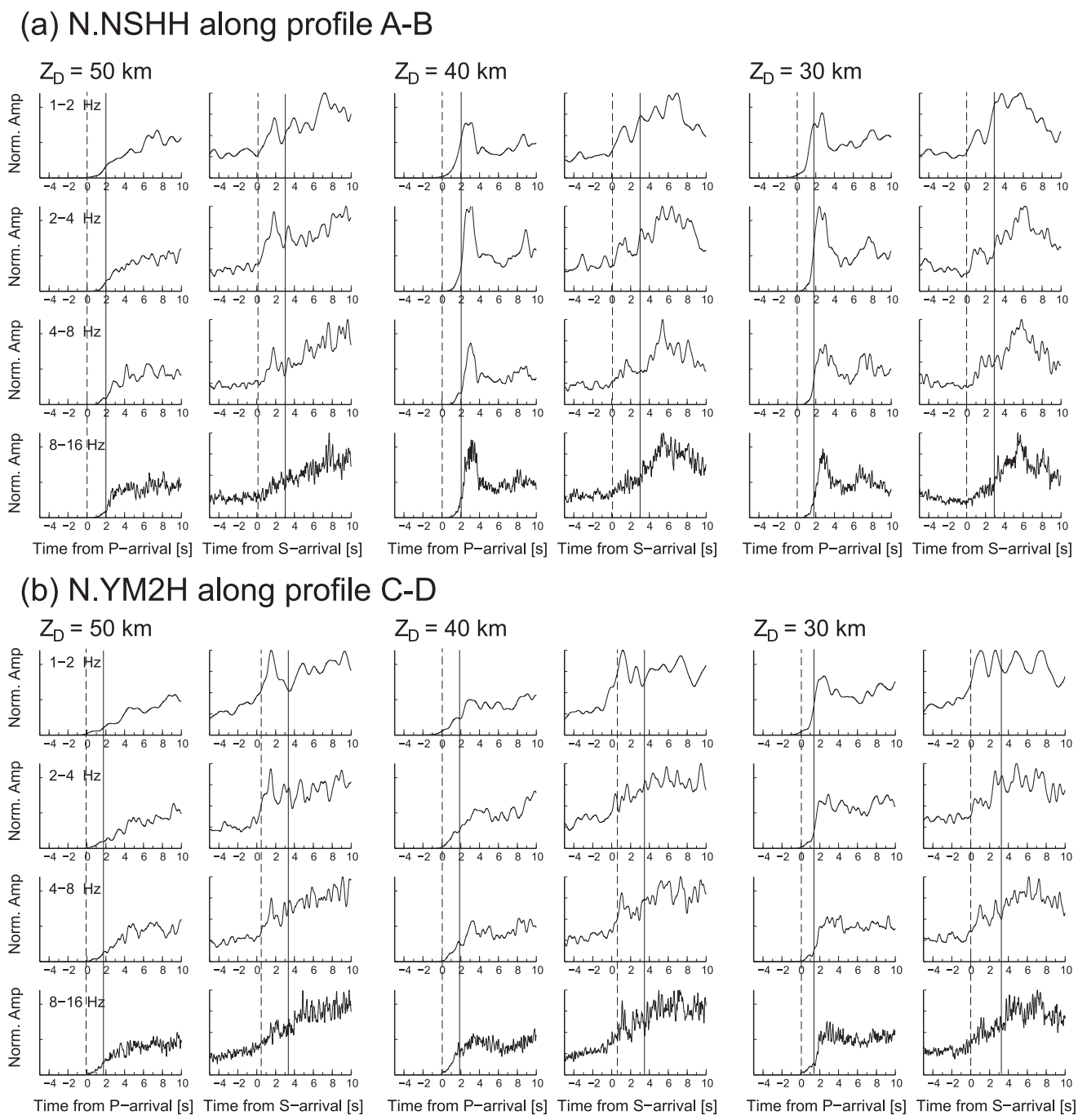


**Figure 13.** Comparison of RMS envelopes at (a) N.NSHH and (b) N.YM2H derived from 2-D simulation results with different $Z_D$ values of 30, 40 and 50 km.

high-frequency trapped *P* and *S* waves. Strong distortion of the trapped wave envelopes was observed in those regions where the Philippine Sea plate exists at shallow depths of less than 15 km. Both 2-D and 3-D FDM simulations demonstrated that the observed spatial variation in envelope shapes was caused by the 3-D configuration of the subducting Philippine Sea plate and by heterogeneous velocity structures in the shallower (<40 km) subducting crust.

In the previous simulations, the observed features of trapped waves were well reproduced by introducing small-scale velocity heterogeneities into the subducting crust at depths of less than 40 km. In this process, a structural change depth of $Z_D = 40$ km was assumed on the basis of previous studies (e.g. Matsubara *et al*. 2005; Takemura *et al*. 2015b). To verify this assumption, we conducted additional 2-D FDM simulations using models with different $Z_D$ values of 30, 40 and 50 km. The model parameters were kept the same as in the previous 2-D simulations (Fig. 9), except that a uniform velocity subducting crust was assumed at depths below $Z_D$.

The simulated RMS envelopes for models with different $Z_D$ values are shown in Fig. 13. From this, it can be seen that the model with $Z_D = 40$ km most accurately reproduced the observed envelope shapes of trapped waves at both stations. The model with $Z_D = 30$ km failed to reproduce the observed spindle features at N.YM2H, while the model with $Z_D = 50$ km was unable to produce pulse-like trapped *P* and *S* waves. These results imply that the small-scale velocity heterogeneities in the subducting crust disappear at 40 km, which is likely due to subduction of the oceanic slab.

In subduction zones of the world, various seismological studies have suggested the occurrence of fluid dehydration from the subducting crust and the formation of a low-velocity anomaly in the mantle wedge (e.g. Kamiya & Kobayashi 2000; Bostock *et al*. 2002; Matsubara *et al*. 2005; Rondenay *et al*. 2008; Hirose *et al*. 2008a,b; Kato *et al*. 2010, 2014; Sodoudi *et al*. 2011). The low-velocity anomaly in the mantle wedge is suggested to be a result of dehydration of the underlying subducting oceanic crust, and it is believed that rich hydrous minerals exist in the subducting crust at shallower depths (e.g. Hacker *et al*. 2003; Kawakatsu & Watada 2007). Thus, we believe that the strong small-scale velocity heterogeneities localized in the subducting crust at depths of less than 40 km may be related to the rich fluids present in this layer. Takahashi *et al.* (2007, 2009) and Takemura & Yoshimoto (2014) also detected strong small-scale velocity heterogeneities in regions characterized by low velocity and high $V_P/V_S$ ratios, which cause strong seismic scattering and amplitude decay. These similar observations, obtained under differing geophysical circumstances, may imply that a crustal medium with a rich fluid content has a high scattering potential for high-frequency seismic waves.

In this study, we investigated the variations in the depths of small-scale velocity heterogeneities in the subducting crust of the Philippine Sea plate, by analysing trapped *P* and *S* waves during intraslab earthquakes. Our results provide new insight into the depth dependence of internal heterogeneities in the subducting crust, as well as their possible geophysical interpretations at shallower depths (<40 km). In future studies, a more detailed analysis of seismogram envelopes, using seismic networks with ocean bottom seismometers, such as DONET (e.g. Nakano *et al*. 2013), could further reveal the characteristics of internal small-scale heterogeneities in the subducting crust.

## ACKNOWLEDGEMENTS

We thank Dr C. Tape, an anonymous reviewer and the editor, Prof Y. Ben-Zion, for constructive comments that improved an earlier draft of this manuscript. We acknowledge the National Research Institute for Earth Science and Disaster Prevention, Japan (NIED) for providing the Hi-net waveform data and CMT solutions from F-net. Computations were conducted on the Earth Simulator (ES2) at the Japan Agency for Marine-Earth Science and Technology (JAMSTEC) under the support of a joint research project: 'Seismic wave propagation and strong ground motion in 3-D heterogeneous structure' conducted by the Earthquake Research Institute, University of Tokyo and the Centre of Earth Information Science and Technology, JAMSTEC. All figures were drawn using the Generic Mapping Tools software package developed by Wessel & Smith (1998).

## REFERENCES

Abers, G., 2005. Seismic low-velocity layer at the top of subducting slabs: observations, predictions and systematics, *Phys. Earth planet. Inter.,* **149,** 7–29.

Abers, G., Plank, T. & Hacker, B., 2003. The wet Nicaraguan slab, *Geophys. Res. Lett.,* **30,** 1098, doi:10.1029/2002GL015649.

Baba, T., Tanioka, Y., Cummins, P.R. & Uhira, K., 2002. The slip distribution of the 1946 Nankai earthquake estimated from tsunami inversion using a new plate model, *Phys. Earth planet. Inter.,* **132,** 59–73.

Ben-Zion, Y., 1998. Properties of seismic fault zone waves and their utility for imaging low-velocity structures, *J. geophys. Res.,* **103,** 12 567–12 585.

Bostock, M.G., Hyndman, R.D., Rondenay, S. & Peacock, S.M., 2002. An inverted continental Moho and serpentinization of the forearc mantle, *Nature,* **417,** 536–538.

Chen, K.H., Kennett, B.L.N. & Furumura, T., 2013. High-frequency waves guided by the subducting plates underneath Taiwan and their association with seismic intensity anomalies, *J. geophys. Res.,* **118,** 1–16.

Frankel, A. & Clayton, R.W., 1986. Finite difference simulations of seismic scattering: implications for the propagation of short-period seismic waves in the crust and models of crustal heterogeneity, *J. geophys. Res.,* **91,** 6465–6489.

Fukao, Y., Hori, S. & Ukawa, M., 1983. A seismological constraint on the depth of basalt-eclogite transition in a subducting oceanic crust, *Nature,* **303,** 413–415.

Fukuyama, E., Ishida, M., Dreger, D.S. & Kawai, H., 1998. Automated seismic moment tensor determination by using on-line broadband seismic waveforms, *Zisin,* **51,** 149–156 (in Japanese with English abstract).

Furumura, T. & Chen, L., 2004. Large scale parallel simulation and visualization of 3-D seismic wavefield using Earth simulator, *Comput. Model. Eng. Sci.,* **6,** 153–168.

Furumura, T. & Kennett, B.L.N., 2005. Subduction zone guided waves and the heterogeneity structure of the subducted plate: Intensity anomalies in northern Japan, *J. geophys. Res.,* **110,** B10302, doi:10.1029/2004JB003486.

Furumura, T., Hong, T.K. & Kennett, B.L.N., 2014. *Lg* wave propagation in the area around Japan: observations and simulations, *Prog. Earth planet. Sci.,* **1,** 10, doi:10.1186/2197-4284-1-10.

Hacker, B.R., Peacock, S.M., Abers, G.A. & Holloway, S.D., 2003. Subduction factory 2. Are intermediate-depth earthquakes in subducting slab linked to metamorphic dehydration reactions?, *J. geophys. Res.,* **108,** 2030, doi:10.1029/2001JB001129.

Hayashida, T., Tajima, F. & Mori, J., 2010. Improved seismic velocity structure in southwestern Japan using pronounced *sP* phase recorded for intra earthquakes, *Bull. seism. Soc. Am.,* **100,** 1928–1939.

Hirose, F., Nakajima, J. & Hasegawa, A., 2008a. Three-dimensional seismic velocity structure and configuration of the Philippine Sea slab in southwestern Japan estimated by double-difference tomography, *J. geophys. Res.,* **133,** B09315, doi:10.1029/2007JB005274.

Hirose, F., Nakajima, J. & Hasegawa, A., 2008b. Three-dimensional velocity structure and configuration of the Philippine Sea Slab beneath Kanto distinct, central Japan, estimated by double-difference tomography, *Zisin,* **60,** 124–138 (in Japanese with English abstract).

Hori, S., 1990. Seismic waves guided by untransformed oceanic crust subducting into the mantle: case of the Kanto distinct, central Japan, *Tectonophysics,* **176,** 355–376.

Hori, S., 2006. Seismic activity associated with the subducting motion of the Philippine Sea plate beneath the Kanto distinct, Japan, *Tectonophysics,* **417,** 85–100.

Iwamori, H. & Zhao, D., 2000. Melting and seismic structure beneath the northeast Japan Arc, *Geophys. Res. Lett.,* **27,** 425–428.

Ji, C., Helmberger, D.V., Wald, D.J. & Ma, K.F., 2003. Slip distribution and dynamic implication of the 1999 Chi-Chi, Taiwan earthquake, *J. geophys. Res.,* **108,** 2412, doi:10.1029/2002JB001764.

Kamiya, S. & Kobayashi, Y., 2000. Seismological evidence for the existence of serpentinized wedge mantle, *Geophys. Res. Lett.,* **27,** 819–822.

Kato, A. *et al.*, 2010. Variation of fluid pressure within the subducting oceanic crust and slow earthquakes, *Geophys. Res. Lett.,* **37,** L14310, doi:10.1029/2010GL043723.

Kato, A., Saiga, A., Takeda, T., Iwasaki, T. & Matsuzawa, T., 2014. Non-volcanic seismic swarm and fluid transportation driven by subduction of the Philippine Sea slab beneath the Kii Peninsula, Japan, *Earth Planets Space,* **66,** 86, doi:10.1186/1880-5981-66-86.

Kawakatsu, H. & Watada, S., 2007. Seismic evidence for deep-water transportation in the mantle, *Science,* **316,** 1468, doi:10.1126/science.1140855.

Kennett, B.L.N. & Furumara, T., 2008. Stochastic waveguide in the lithosphere: Indonesian subduction zone to Australian craton, *Geophys. J. Int.,* **172,** 363–382.

Kirby, S., Engdahl, R.E. & Denlinger, R., 1996. Intermediate-depth intraslab earthquakes and arc volcanism as physical expressions of crustal and

uppermost mantle metamorphism in subducting slabs, in *Subduction: Top to Bottom,* Geophys. Monogr. Ser., Vol. 96, pp. 195–214, eds Bebout, G.E. *et al.*, AGU, Washington, DC.

Koketsu, K., Miyake, H., Fujiwara, H. & Hashimoto, T., 2008. Progress towards a Japan integrated velocity structure model and long-period ground motion hazard map, in *Proceedings of the 14th World Conference on Earthquake Engineering,* Beijing, China, October 12–17.

Koketsu, K., Miyake, H. & Suzuki, H., 2012. Japan integrated velocity structure model version 1, in *Proceedings of the 15th World Conference on Earthquake Engineering,* Lisbon, Portugal, September 24–28.

Kumar, P. & Kawakatsu, H., 2011. Imaging the seismic lithosphere-asthenosphere boundary of the oceanic plate, *Geochem. Geophys. Geosyst.,* **12,** Q01006, doi:10.1029/2010GC003358.

Kuwatani, T., Okamoto, A. & Toriumi, M., 2011. Thermodynamic forward modeling of progressive dehydration reactions during subduction of oceanic crust under greenschist facies conditions, *Earth planet. Sci. Lett.,* **307,** 9–18.

Lewis, M.A. & Ben-Zion, Y., 2010. Diversity of fault zone damage and trapping structures in the Parkfield section of the San Andreas Fault from comprehensive analysis of near fault seismograms, *Geophys. J. Int.,* **183,** 1579–1595.

Liu, X. & Zhao, D., 2015. Seismic attenuation tomography of the southwestern Japan arc: new insight into subduction dynamics, *Geophys. J. Int.,* **201,** 135–156.

Maeda, T. & Furumura, T., 2013. FDM simulation of seismic waves, ocean acoustic waves, and tsunamis based on tsunami-coupled equation of motion, *Pure appl. Geophys.,* **170,** 109–127.

Maeda, T., Obara, K., Furumura, T. & Saito, T., 2011. Interference of long-period seismic wavefield observed by the dense Hi-net array in Japan, *J. geophys. Res.,* **116,** B10303, doi:10.1029/2011JB008464.

Martin, S. & Rietbrock, A., 2006. Guided waves subduction zones: dependencies on slab geometry, receiver locations and earthquake sources, *Geophys. J. Int.,* **167,** 693–704.

Matsubara, M., Hayashi, H., Obara, K. & Kasahara, K., 2005. Low-velocity oceanic crust at the top of the Philippine Sea and Pacific plates beneath the Kanto region, central Japan, imaged by seismic tomography, *J. geophys. Res.,* **110,** B12304, doi:10.1029/2005JB003673.

Mavroeidis, G.P. & Papageorgiou, A.S., 2003. A mathematical representation of near-field ground motions, *Bull. seism. Soc. Am.,* **93,** 1099–1131.

Miyoshi, T. & Ishibashi, K., 2007. Distinct regional phases on seismograms of intraslab earthquakes within the Philippine Sea plate beneath southwestern Japan, *Zisin,* **60,** 101–106 (in Japanese with English abstract).

Miyoshi, T., Saito, T. & Shiomi, K., 2012. Waveguide effects within the Philippine Sea slab beneath southwest Japan inferred from guided SP converted waves, *Geophys. J. Int.,* **189,** 1075–1084.

Mizoue, T. & Nishigami, K., 2006. Deep structure of the Nojima fault, southwest Japan, estimated from borehole observation of fault-zone trapped waves, *Tectonophysics,* **417,** 231–247.

Nakajima, J., Hirose, F. & Hasegawa, A., 2009a. Seismotectonics beneath the Tokyo metropolitan area, Japan: effect of slab-slab contact and overlap on seismicity, *J. geophys. Res.,* **114,** B08309, doi:10.1029/2008JB006101.

Nakajima, J., Tsuji, Y. & Hasegawa, A., 2009b. Seismic evidence for thermally-controlled dehydration reaction in subducting oceanic crust, *Geophys. Res. Lett.,* **36,** L03303, doi:10.1029/2008GL036865.

Nakano, M., Nakamura, T., Kamiya, S., Ohori, M. & Kaneda, Y., 2013. Intensive seismic activity around the Nankai trough revealed by DONET ocean-floor seismic observations, *Earth Planets Space,* **65,** 5–15.

Obara, K. & Maeda, T., 2009. Reverse propagation of T waves from the Emperor Seamount Chain, *Geophys. Res. Lett.,* **36,** L08304, doi:10.1029/2009GL037454.

Okada, Y., Kasahara, K., Hori, S., Obara, K., Sekiguchi, S., Fujiwara, H. & Yamamoto, A., 2004. Recent progress of seismic observation networks in Japan: Hi-net, F-net, K-NET and KiK-net, *Earth Planets Space,* **56,** 15–28.

Okal, E.A., 2008. The generation of *T* waves by earthquakes, *Adv. Geophys.,* **49,** 1–65.

Peacock, S.M., 1993. Large-scale hydration of the lithosphere above subducting slabs, *Chem. Geol.,* **108,** 49–59.

Peng, Z., Ben-Zion, Y., Michael, A.J. & Zhu, L.P., 2003. Quantitative analysis of seismic fault zone waves in the rupture zone of the Landers, 1992, California earthquake: evidence for a shallow trapping structure, *Geophys. J. Int.,* **155,** 1021–1041.

Robertsson, J., 1994. Viscoelastic finite-difference modeling, *Geophys,* **59,** 1444–1456.

Rondenay, S., Abers, G.A. & van Keken, P.E., 2008. Seismic imaging of subduction zone metamorphism, *Geology,* **36,** 275–278.

Sato, H., 1984. Attenuation and envelope formation of three-component seismograms of small local earthquakes in randomly inhomogeneous lithosphere, *J. geophys. Res.,* **89,** 1221–1241.

Sato, H., Fehler, M. & Maeda, T., 2012. *Seismic Wave Propagation and Scattering in the Heterogeneous Earth Structure,* 2nd edn, Springer-Verlag.

Shiina, T., Nakajima, J. & Matsuzawa, T., 2013. Seismic evidence for high pore pressures in the oceanic crust: implication for fluid-related embrittlement, *Geophys. Res. Lett.,* **40,** 2006–2010.

Shiina, T., Nakajima, J., Toyokuni, G. & Matsuzawa, T., 2014. Guided wave observations and evidence for the low-velocity subducting crust beneath Hokkaido, northern Japan, *Earth Planets Space,* **66,** 69, doi:10.1186/1880-5981-66-69.

Shiomi, K., Obara, K., Aoi, S. & Kasahara, K., 2003. Estimation of the azimuth of the Hi-net and KiK-net borehole seismometers, *Zisin,* **56,** 99–110 (in Japanese with English abstract).

Sodoudi, F., Yuan, X., Asch, G. & Kind, R., 2011. High-resolution image of the geometry and thickness of the subducting Nazca lithosphere beneath northern Chile, *J. geophys. Res.,* **116,** B04302, doi:10.1029/2010JB007829.

Takahashi, T., Sato, H., Nishimura, T. & Obara, K., 2007. Strong inhomogeneity beneath Quaternary volcanoes revealed from the peak delay analysis of S-wave seismograms of microearthquakes in northeastern Japan, *Geophys. J. Int.,* **168,** 90–99.

Takahashi, T., Sato, H., Nishimura, T. & Obara, K., 2009. Tomographic inversion of the peak delay times to reveal random velocity fluctuations in the lithosphere: method and application to northeastern Japan, *Geophys. J. Int.,* **178,** 1437–1455.

Takaoka, H. *et al.*, 2012. Three-dimensional attenuation structure beneath the Tokai region, central Japan derived using local earthquake spectra, *Zisin,* **65,** 175–187 (in Japanese with English abstract).

Takemura, S. & Furumura, T., 2013. Scattering of high-frequency *P* wavefield derived from by dense Hi-net array observations in Japan and computer simulations of seismic wave propagations, *Geophys. J. Int.,* **193,** 421–436.

Takemura, S. & Yoshimoto, K., 2014. Strong seismic wave scattering in the low-velocity anomaly associated with subduction of oceanic plate, *Geophys. J. Int.,* **197,** 1016–1032.

Takemura, S., Furumura, T. & Saito, T., 2009. Distortion of the apparent S-wave radiation pattern in the high-frequency wavefield: Tottori-ken Seibu, Japan, earthquake of 2000, *Geophys. J. Int.,* **178,** 950–961.

Takemura, S., Furumura, T. & Maeda, T., 2015a. Scattering of high-frequency seismic waves caused by irregular surface topography and small-scale velocity inhomogeneity, *Geophys. J. Int.,* **201,** 459–474.

Takemura, S., Yoshimoto, K. & Tonegawa, T., 2015b. Velocity increase in the uppermost oceanic crust of the Philippine Sea plate beneath the Kanto region due to dehydration inferred from high-frequency *P* waves, *Earth Planets Space,* **67,** 41, doi:10.1186/s40623-015-0210-6.

Tatsumi, Y., 1989. Migration of fluid phases and genesis of basalt magmas in subduction zones, *J. geophys. Res.,* **94,** 4697–4707.

Tonegawa, T. & Helffrich, G., 2012. Basal reflector under the Philippine Sea Plate, *Geophys. J. Int.,* **189,** 659–668.

Tsuji, Y., Nakajima, J. & Hasegawa, A., 2008. Tomographic evidence for hydrated oceanic crust of the Pacific slab beneath northeastern Japan: implications for water transportation in subduction zones, *Geophys. Res. Lett.,* **35,** L14308, doi:10.1029/2008GL034461.

Wessel, P. & Smith, W.H.F., 1998. New, improved version of generic mapping tools released, *EOS, Trans. Am. geophys. Un.,* **79**(47), 579, doi:10.1029/98EO00426.

Yabe, S., Baltay, A., Ide, S. & Beroza, G., 2014. Seismic-wave attenuation determined from tectonic tremor in multiple subduction zones, *Bull. seism. Soc. Am.,* **104,** doi:10.1785/0120140032.